Optimizing multifunctional materials: Design of microstructures for maximized stiffness and fluid permeability

James K. Guest [a,*], Jean H. Prévost [b]

[a] *Department of Civil Engineering, Johns Hopkins University, 3400 N. Charles Street, 210 Latrobe Hall, Baltimore, MD 21218, United States*
[b] *Department of Civil and Environmental Engineering, Princeton University, Princeton, NJ 08544, United States*

Abstract

Topology optimization is used to systematically design periodic materials that are optimized for multiple properties and prescribed symmetries. In particular, mechanical stiffness and fluid transport are considered. The base cell of the periodic material serves as the design domain and the goal is to determine the optimal distribution of material phases within this domain. Effective properties of the material are computed from finite element analyses of the base cell using numerical homogenization techniques. The elasticity and fluid flow inverse homogenization design problems are formulated and existing techniques for overcoming associated numerical instabilities and difficulties are discussed. These modules are then combined and solved to maximize bulk modulus and permeability in periodic materials with cubic elastic and isotropic flow symmetries. The multiphysics problem is formulated such that the final design is dependent on the relative importance, or weights, assigned by the designer to the competing stiffness and flow terms in the objective function. This allows the designer to tailor the microstructure according to the materials' future application, a feature clearly demonstrated by the presented results. The methodology can be extended to incorporate other material properties of interest as well as the design of composite materials.
© 2006 Elsevier Ltd. All rights reserved.

Keywords: Topology optimization; Inverse homogenization; Multiphysics; Length scale; Finite element method

1. Introduction

Development of optimized multifunctional materials is of great interest from technological and theoretical viewpoints to all engineering fields. This paper designs such materials computationally using the method of topology optimization. In particular, three-dimensional periodic porous materials are simultaneously optimized for mechanical stiffness and fluid permeability while achieving prescribed elastic and flow symmetries. The design optimization problem is formulated such that the designer may manipulate the microstructure by assigning weights, or measures of relative importance, to the competing stiffness and permeability terms in the

* Corresponding author. Tel.: +1 410 516 3923; fax: +1 410 516 7473.
 E-mail addresses: jkguest@jhu.edu (J.K. Guest), prevost@princeton.edu (J.H. Prévost).

objective function. The designer selects these weights based on the materials future use, thus allowing the microstructure to be tailored according to its specific application.

Design of material microstructures using topology optimization is a relatively young field. The underlying idea is that the microstructure of material can be viewed as a small structure, allowing for the application of structural topology optimization methods developed for macroscopic design problems (Sigmund, 1994a; Bendsøe and Sigmund, 2003). Microstructural behavior is linked to macroscopic properties by homogenization theory, which provides a means for computing the effective (average) properties of a material via analysis of a single realization, or base cell. Homogenization eliminates the need to analyze a bulk of the material at the microscopic scale, an enormous and potentially infeasible computational task. The design of materials is then an inverse homogenization problem: find the optimal base cell design that yields desired effective properties.

Topology optimization seeks to determine the optimal distribution of material phases in a given design domain and hence it is well suited for solving the inverse homogenization problem. In typical two-phase solid-void design problems, the approach reduces to determining whether or not material is present at each point in space within the base cell. The material distribution function is traditionally denoted as $\rho(\mathbf{x})$, where $\rho(\mathbf{x}) = 1$ indicates solid material present at location $\mathbf{x}$ and $\rho(\mathbf{x}) = 0$ indicates the presence of a void. Bendsøe and Kikuchi (1988) provided a numerical implementation of the material distribution approach where the design domain is discretized using finite elements, with each element having a volume fraction, or relative density, ρ^e that indicates the presence (or lack) of material within the element. Phase is constant inside each element and thus connectivity of the solid elements defines topology.

The inverse homogenization problem was first solved with topology optimization by Sigmund (1994a,b, 1995) using truss and frame modeled base cells to design minimum weight topologies with prescribed elastic properties, including negative Poisson's ratio. It has since been used to design minimum weight materials with prescribed thermoelastic properties (Sigmund, 1994a), materials with extreme elastic or thermal expansion properties (Sigmund and Torquato, 1997), piezocomposites (Sigmund et al., 1998), and materials with extreme fluid transport properties (Guest, 2005; Guest and Prévost, under review).

An area of topology optimization that remains relatively unexplored is the design of multifunctional materials. The above-mentioned works have focused on optimizing a single property, often while requiring a lower bound on a competing property. For example, Sigmund and Torquato (1997) minimized the isotropic thermal strain coefficient while enforcing a lower bound on effective bulk modulus. Recently, Torquato et al. (2002, 2003) used two-phase composite materials to maximize the simultaneous transport of heat and electricity, properties that are both governed by scalar equations. The material phases were selected such that one phase has high thermal conductivity but low electrical conductivity and the other phase has low thermal conductivity but high electrical conductivity. The effective scalar properties were summed in the objective function and the solution was found to be a triply periodic minimal surface. By mathematical analogy, the results apply to any pair of the following effective properties: electrical conductivity, thermal conductivity, dielectric constant, and magnetic permeability (Torquato et al., 2002).

The goal of this work is to design periodic multifunctional materials for maximum effective elastic stiffness and fluid permeability. These properties are competing, as stiffness desires large quantities of solid while permeability desires large holes in the topology. We formulate the problem such that the final design is dependent on the weight assigned to the stiffness and transport terms in the objective function, thereby allowing the designer to tailor the microstructure according to its future use.

While periodic materials have been designed for either maximum effective stiffness or maximum fluid permeability, the combined problem simultaneously optimizing both properties is extraordinarily complex and has yet to be attempted. Vector equations govern both properties and the problem must be formulated and solved in three dimensions to be meaningful. This yields a complex system of governing equations in the optimization problem. To simplify matters, we will assume deformations are uncoupled from fluid velocities and, therefore, will not consider materials with low void ratios and relatively thin walls susceptible to flow-induced deformation. Although the presented methodology is applicable to such materials, the computational requirements are more intensive.

The problem is complicated further by known numerical instabilities in the maximum stiffness problem (mesh dependence and checkerboard patterns) and numerical difficulties in the flow optimization problem (simulating the moving-boundary no-slip condition). We solve the homogenization equations numerically

using finite elements and circumvent the numerical issues using techniques developed by the authors for macroscopic design problems. Solutions to the proposed multi-objective design problem demonstrate that a wide-range of material designs are obtained by varying the weight assigned to the competing properties in the objective function.

The layout of the paper is as follows. The elastic and fluid homogenization equations are given in Section 2 and the inverse homogenization problem is formulated in Section 3. Section 4 summarizes numerical issues associated with the maximum stiffness and fluid flow problems and the techniques used for circumventing these issues. The optimization algorithm and results are presented in Sections 5 and 6, respectively. Concluding remarks are given in Section 7.

2. The homogenization equations

In this work we consider periodic materials characterized by a single base cell, denoted as Y. The base cell is repeated to form the periodic material. Homogenization is performed numerically using finite elements, and periodic boundary conditions are implemented by assigning the same equation number to the degrees of freedom of opposing nodes. This is the simplest way to enforce the periodic boundary conditions as standard finite element assembly and solution routines can be used without modification.

2.1. Elastic homogenization

The goal of elastic homogenization is to determine the effective stiffness tensor $\mathbf{C}^{\mathrm{H}}$ of a material, where the constitutive equation for linear elastic behavior is assumed:

$$\boldsymbol{\sigma} = \mathbf{C}^{\mathrm{H}}\boldsymbol{\varepsilon} \tag{1}$$

where $\boldsymbol{\sigma}$ and $\boldsymbol{\varepsilon}$ are the stress and strains fields, respectively.

As developed in Bensoussan et al. (1978) and Sanchez-Palencia (1980), the effective elasticity tensor of a periodic material can be expressed in energy form in the following manner:

$$C_{pqrs}^{\mathrm{H}}\varepsilon_{pq}^{o(kl)}\varepsilon_{rs}^{o(ij)} = \frac{1}{|Y|}\int_Y C_{pqrs}\big(\varepsilon_{pq}^{o(kl)} - \varepsilon_{pq}^*(x^{kl})\big)\big(\varepsilon_{rs}^{o(ij)} - \varepsilon_{rs}^*(x^{ij})\big)\,\mathrm{d}Y \tag{2}$$

where C_{pqrs} is the elasticity tensor of the solid (matrix) material, $\varepsilon_{pq}^{o(kl)}$ are the test strain fields, $\varepsilon_{pq}^*(x^{kl})$ are the fluctuation strains caused by the inhomogeneous base cell defined through the strain–displacement relations $\varepsilon_{pq}^*(\boldsymbol{x}^{kl}) = \frac{1}{2}\big(\frac{\partial x_p^{kl}}{\partial y_q} + \frac{\partial x_q^{kl}}{\partial y_p}\big)$, and the displacement fields $\mathbf{x}^{kl}$ is found through solution to the following base cell problem:

$$\int_Y C_{ijpq}\frac{\partial x_p^{kl}}{\partial y_q}\frac{\partial v_i}{\partial y_j}\,\mathrm{d}Y = \int_Y C_{ijpq}\varepsilon_{pq}^{o(kl)}\frac{\partial v_i}{\partial y_j}\,\mathrm{d}Y \quad \forall v \in \widetilde{V}$$
$$\widetilde{V} = \{v : v \text{ is } Y\text{-periodic}\} \tag{3}$$

The test strain fields $\varepsilon_{pq}^{o(kl)}$ are chosen as unit vectors and symmetry is used to reduce the number of test strain fields in three-dimensional elasticity from nine to six (three normal and three shear strain cases).

The homogenization is performed numerically using finite element analysis. Following the work of Guedes and Kikuchi (1990), the base cell is discretized and, after integration over each element and substituting the definitions of the unit strain tensors into the left-hand side of Eq. (2), the homogenized elasticity tensor is written using standard finite element notation as

$$C_{ijkl}^{\mathrm{H}} = \frac{1}{|Y|}\sum_{e \in Y}\big(\mathbf{d}_o^{e(ij)} - \mathbf{d}^{e(ij)}\big)^{\mathrm{T}}\mathbf{k}^e(\rho^e)\big(\mathbf{d}_o^{e(kl)} - \mathbf{d}^{e(kl)}\big) \tag{4}$$

where $\mathbf{k}^e(\rho^e)$ is the stiffness matrix of element e expressed as a function of the element volume fraction ρ^e, $\mathbf{d}_o^{e(ij)}$ is the vector of nodal displacements for element e corresponding to the unit test strain field $\varepsilon^{o(ij)}$, and $\mathbf{d}^{e(ij)}$ is the vector of nodal displacements for element e related to the strain field $\varepsilon^*(\mathbf{x}^{ij})$. The displacements $\mathbf{d}^{(ij)}$ are unknown and are found by solving the matrix problem

$$\mathbf{K}(\rho^e)\mathbf{d}^{(ij)} = \mathbf{f}^{(ij)}$$
$$\mathbf{d}^{(ij)} \text{is } Y\text{-periodic} \tag{5}$$

where $\mathbf{K}(\rho^e)$ is the global stiffness matrix assembled (A) from the element stiffness matrices and the nodal forces $\mathbf{f}^{(ij)}$ result from the unit test strain field (ij) and are computed by

$$\mathbf{f}^{(ij)} = \underset{e}{A}\, \mathbf{k}^e(\rho^e)\mathbf{d}_o^{e(ij)} \tag{6}$$

Note that a uniform distribution of material yields a zero nodal force vector and consequently a zero nodal displacement vector $\mathbf{d}^{(ij)}$. The effective stiffness then equals the stiffness of the matrix material, i.e., $\mathbf{C}^H = \mathbf{C}$.

Boundary conditions are applied to the base cell boundaries to prevent rigid body motion and impose the unit strain field. In the two-dimensional case, for example, displacements in the direction normal to the boundary are constrained for the normal test strain fields (Eqs. (11) and (22)), and in the direction parallel to the boundary for the shear test strain field (Eq. (12)). The reader is referred to Hassani and Hinton (1998) for details and figures regarding the base cell boundary conditions. Periodic boundary conditions are applied to the unrestricted nodes on the boundary as previously discussed.

2.2. Homogenization of Stokes flow

Consider an incompressible viscous fluid that flows slowly through a porous medium. On the macroscopic scale, flow through the material is governed by Darcy's law:

$$\mathbf{U} = -\frac{1}{\mu}\mathbf{K}^H \cdot (\nabla p_0 - \rho_f \mathbf{b}) \tag{7}$$

where $\mathbf{U}$ is the vector of average fluid velocities, μ is the viscosity, $\mathbf{K}^H$ is the permeability tensor, ∇p_0 is the applied pressure gradient, ρ_f is the fluid mass density, and $\mathbf{b}$ is the body force vector per unit mass. On the microscopic scale, fluid flow through the void channels Ω_f of the porous material is governed by Stokes equations:

$$\mu\nabla^2\mathbf{u} - \nabla p = -\rho_f\mathbf{b} \quad \text{in } \Omega_f$$
$$\nabla \cdot \mathbf{u} = 0 \quad \text{in } \Omega_f \tag{8}$$
$$\mathbf{u} = \mathbf{0} \quad \text{on } \Gamma_s$$

where $\mathbf{u}$ are the local velocities and p is the pressure. The third equation represents the no-slip condition along the solid–fluid interface Γ_s.

Sanchez-Palencia (1980), operating in the context of periodic materials, was the first to derive Darcy's law from Stokes equations using homogenization. Defining a system of local coordinates $\mathbf{y}$ in the base cell Y, the homogenized effective permeability tensor $\mathbf{K}^H$ of a porous medium can be expressed as an ensemble average of fluid velocities in the base cell as follows:

$$\mathbf{K}^H = \langle \mathbf{w}(\mathbf{y})\rangle \tag{9}$$

where $\langle\,\rangle$ represents the ensemble average and $\mathbf{w}$ is the characteristic flow field, or fluid velocity tensor in the base cell, found by solving the following scaled Stokes flow equations:

$$\nabla^2\mathbf{w}(\mathbf{y}) - \nabla\boldsymbol{\pi}(\mathbf{y}) = -\mathbf{I} \quad \mathbf{y} \in \Omega_f(Y)$$
$$\nabla \cdot \mathbf{w}(\mathbf{y}) = 0 \quad \mathbf{y} \in \Omega_f(Y)$$
$$\mathbf{w}(\mathbf{y}) = \mathbf{0} \quad \mathbf{y} \in \Gamma_s(Y) \tag{10}$$
$$\mathbf{w} \text{ is } Y\text{-periodic}$$

where $\boldsymbol{\pi}$ is the characteristic pressure field and $\mathbf{I}$ is the second-order Identity tensor. The term w_{ij} of the flow tensor $\mathbf{w}$ can thus be described as the velocity in the ith direction under a unit pressure gradient in the jth direction, and π_j is the jth component of the scaled pressure. The size of the identity matrix is the number of spatial dimensions d considered. The reader is referred to Sanchez-Palencia (1980) and Torquato (2002) for further detail regarding derivation of the fluid homogenization equations.

As we will be using homogenization in the context of optimization, it is useful to express effective permeability in terms of power. Following Torquato (2002), the homogenized permeability of an ergodic medium can be expressed as

$$\mathbf{K}^{\mathrm{H}} = \langle \mathbf{w} \rangle = -\langle \mathbf{w} \cdot \nabla^2 \mathbf{w} \rangle = \langle \nabla \mathbf{w} : \nabla \mathbf{w} \rangle \tag{11}$$

For convenience in future notation, let us introduce a superscript to Eq. (10) to isolate the spatial dimensions:

$$\nabla^2 \mathbf{w}^{(i)}(\mathbf{y}) - \nabla \pi^{(i)}(\mathbf{y}) = -\mathbf{e}^{(i)} \quad \mathbf{y} \in \Omega_{\mathrm{f}}(Y)$$
$$\nabla \cdot \mathbf{w}^{(i)}(\mathbf{y}) = 0 \quad \mathbf{y} \in \Omega_{\mathrm{f}}(Y) \tag{12}$$
$$\mathbf{w}^{(i)}(\mathbf{y}) = \mathbf{0} \quad \mathbf{y} \in \Gamma_{\mathrm{s}}(Y)$$

for $i = 1, d$, where the velocity vector $\mathbf{w}^{(i)}$, scalar pressure $\pi^{(i)}$, and body force vector $\mathbf{e}^{(i)}$ associated with direction case i are related to the tensors $\mathbf{w}$, $\boldsymbol{\pi}$, and $\mathbf{I}$ by

$$w_j^{(i)} = w_{ji}, \quad \pi^{(i)} = \pi_i, \quad e_j^{(i)} = \delta_{ji} \tag{13}$$

where δ is the Kronecker delta.

The system of Stokes flow equations (12) is solved numerically in the mixed formulation using stabilized finite elements to circumvent the Babuska–Brezzi condition (Babuska, 1971; Brezzi, 1974). Specifics regarding the stabilization will be discussed in Section 4. Let us give the matrix form of the stabilized Stokes flow problem as

$$\begin{bmatrix} \mathbf{K}_{\mathrm{s}} & -\mathbf{G}_{\mathrm{s}} \\ \mathbf{L}_{\mathrm{s}} + \mathbf{G}_{\mathrm{s}}^{\mathrm{T}} & \mathbf{M}_{\mathrm{s}} \end{bmatrix} \begin{bmatrix} \mathbf{w}^{(i)} \\ \pi^{(i)} \end{bmatrix} = \begin{bmatrix} \mathbf{f}_{\mathrm{s}}^{(i)} \\ \mathbf{h}_{\mathrm{s}} \end{bmatrix} \quad \text{for } i = 1, d \tag{14}$$

where $\mathbf{K}_{\mathrm{s}}$ is the viscosity stiffness matrix, $\mathbf{G}_{\mathrm{s}}$ is the gradient matrix, $\mathbf{G}_{\mathrm{s}}^{\mathrm{T}}$ is the divergence matrix, $\mathbf{L}_{\mathrm{s}}$ is the consistency matrix, $\mathbf{M}_{\mathrm{s}}$ is the stabilization matrix, and $\mathbf{f}_{\mathrm{s}}^i$ and $\mathbf{h}_{\mathrm{s}}$ are the nodal forces resulting from body forces and boundary conditions. Note that only the body forces in vector $\mathbf{f}_{\mathrm{s}}^{(i)}$ change with each loading case. The subscript 's' has been added to the above terms to emphasize Stokes flow for clarity in future use.

Consequently, the computation of the effective permeability tensor is expressed in finite element notation as

$$\mathbf{K}^{\mathrm{H}} = [K_{ij}^{\mathrm{H}}] = [\langle w_j^{(i)} \rangle] = \frac{1}{|Y|} \mathbf{w}^{(i)\mathrm{T}} \mathbf{K}_{\mathrm{s}} \mathbf{w}^{(j)} = \frac{1}{|Y|} \sum_{e \in \Omega} (\mathbf{w}^{(i)})^{e\mathrm{T}} \mathbf{k}_{\mathrm{s}}^e (\mathbf{w}^{(j)})^e \tag{15}$$

where $\mathbf{k}_{\mathrm{s}}^e$ is element viscosity stiffness matrix and $(\mathbf{w}^i)^e$ is the nodal velocity vector of element e for load case i.

3. Inverse homogenization problem formulation

Homogenization theory allows us to compute effective properties of the bulk material given the topology of a base cell. We seek to design materials, and thus must formulate and solve an inverse homogenization problem: find the optimal base cell topology that yields desired effective properties. The characteristic base cell is the design domain and a material distribution problem must be solved. As in traditional structural optimization, each element in the base cell possesses a volume fraction ρ^e, or relative density, that indicates what phase is present in the elemental domain, where $\rho^e = 1$ represents material present (e is a solid element) and $\rho^e = 0$ represents fluid present (e is a void element). Connectivity of the solid elements defines topology, which in turn dictates stiffness and fluid velocities. Therefore, ρ^e is traditionally the design variable (see e.g., Bendsøe and Sigmund, 2003). As previously mentioned, we will assume fluid velocities are uncoupled from matrix deformations to simplify computations.

As discussed in the introduction, the multi-objective approach taken here allows the designer to assign different weights, or measures of importance, to the stiffness and transport terms in the objective function according to the materials intended future use. These weights then influence the final design.

The topology optimization problem is formulated with constraints including prescribed elastic and fluid flow symmetries, the homogenization equations, lower (V_{L}) and upper (V_{U}) bounds on the available volume of material, and bounds on the element volume fraction ρ^e. As reported in other inverse homogenization

works (Sigmund and Torquato, 1997; Sigmund et al., 1998; Guest, 2005), we have found the problem easier to solve when prescribed symmetry constraints are enforced using a penalty term in the objective function. Further, we will be using a nested-loop approach where design and state variables are computed independently, potentially leading to infeasible designs during optimization iterations. Expressing these symmetry constraints as penalty functions, however, allows for the use of feasible region optimization methods. The topology optimization problem consequently takes the following form:

$$\max_{\rho^e,\mathbf{d},\mathbf{w},\boldsymbol{\pi}} \quad \alpha_{\mathrm{stiff}}f_{\mathrm{stiff}}(\rho^e,\mathbf{d}) + \alpha_{\mathrm{perm}}f_{\mathrm{perm}}(\rho^e,\mathbf{w}) - \left(w_{\mathrm{stiff}}\,error_{\mathrm{stiff}}(\rho^e,\mathbf{d}) + w_{\mathrm{perm}}\,error_{\mathrm{perm}}(\rho^e,\mathbf{w})\right)$$

$$\text{subject to} \quad V_{\mathrm{L}} \leqslant \sum_{e \in \Omega} \rho^e v^e \leqslant V_{\mathrm{U}}$$

$$\mathbf{K}(\rho^e)\mathbf{d}^{(ij)} = \mathbf{f}^{(ij)}(\rho^e)$$

$$\begin{bmatrix} \mathbf{K}_{\mathrm{s}}(\rho^e) & -\mathbf{G}_{\mathrm{s}}(\rho^e) \\ \mathbf{L}_{\mathrm{s}}(\rho^e) + \mathbf{G}_{\mathrm{s}}^{\mathrm{T}}(\rho^e) & \mathbf{M}_{\mathrm{s}}(\rho^e) \end{bmatrix} \begin{bmatrix} \mathbf{w}^{(i)} \\ \pi^{(i)} \end{bmatrix} = \begin{bmatrix} \mathbf{f}_{\mathrm{s}}^{(i)}(\rho^e) \\ \mathbf{h}_{\mathrm{s}}(\rho^e) \end{bmatrix} \quad \text{for } i,j = 1,d \tag{16}$$

$$\mathbf{w}^{(i)} = \mathbf{0} \quad \forall \mathbf{y} \in \Gamma_{\mathrm{s}}$$

$$\mathbf{d}^{(ij)}, \mathbf{w}^{(i)} \text{ is } Y\text{-periodic}$$

$$\rho^e = \{\rho_{\mathrm{min}}^e, 1\} \quad \forall e \in \Omega$$

where α_{stiff} and α_{perm} are the weights assigned to the stiffness and permeability objectives f_{stiff} and f_{perm}, respectively, selected such that $\alpha_{\mathrm{stiff}} + \alpha_{\mathrm{perm}} = 1$, and w_{stiff} and w_{perm} are the weights assigned to the elastic and flow symmetry penalty functions $error_{\mathrm{stiff}}$ and $error_{\mathrm{perm}}$, respectively. To avoid local minima, w_{stiff} and w_{perm} are initially set to a small number (e.g., 1.0) and are increased as the algorithm progresses. The variable v^e is the volume of element e and ρ_{min}^e is a small positive number to avoid singularity of the elastic global stiffness matrix $\mathbf{K}$, necessary as element stiffness is initially set proportional to the element volume fraction by

$$\mathbf{k}^e(\rho^e) = \rho^e \mathbf{k}_0^e \tag{17}$$

where $\mathbf{k}_0^e$ is the element stiffness matrix of a solid element. Although it will be discussed in Section 4, for completeness let us simply say that void elements have Stokes flow stiffness while solid elements carry no-slip nodal boundary conditions.

3.1. The stiffness term in the objective function

The elastic property we choose to maximize is bulk modulus B, a material's resistance to volumetric strain. This is measure of stiffness and a property that is often optimized in literature (Sigmund and Torquato, 1997; Sigmund, 2000; Bendsøe and Sigmund, 2003). Assuming cubic or isotropic symmetry, the bulk modulus of a material can be expressed in terms of the three-dimensional effective elasticity tensor as

$$B^{\mathrm{H}} = \frac{1}{3}\left(\frac{1}{3}\left(C_{11}^{\mathrm{H}} + C_{22}^{\mathrm{H}} + C_{33}^{\mathrm{H}}\right) + \frac{2}{3}\left(C_{12}^{\mathrm{H}} + C_{13}^{\mathrm{H}} + C_{23}^{\mathrm{H}}\right)\right) \tag{18}$$

The functions f_{stiff} and f_{perm} are normalized to improve scaling of the objective function. We simply use the maximum values obtained from solving the individual optimization problems. In other words, the elastic normalization term B^* is the bulk modulus when problem (16) is solved with $\alpha_{\mathrm{stiff}} = 1$ (and without normalization). Alternatively, each normalization term could be selected as the theoretical upper bound on the property that is being optimized. Note that weighting schemes in multi-objective optimization typically carry only internal meaning to the user and thus normalization is not required.

The elastic stiffness function to be optimized is therefore given by

$$f_{\mathrm{stiff}}(\rho^e,\mathbf{d}) = \frac{B^{\mathrm{H}}(\rho^e,\mathbf{d})}{B^*} \tag{19}$$

We will design cubic symmetric materials in three dimensions, requiring the effective stiffness matrix to take the following form:

$$\mathbf{C}_{\text{cubic}} = \begin{bmatrix} C_{11} & C_{12} & C_{12} & 0 & 0 & 0 \\ C_{12} & C_{11} & C_{12} & 0 & 0 & 0 \\ C_{12} & C_{12} & C_{11} & 0 & 0 & 0 \\ 0 & 0 & 0 & C_{44} & 0 & 0 \\ 0 & 0 & 0 & 0 & C_{44} & 0 \\ 0 & 0 & 0 & 0 & 0 & C_{44} \end{bmatrix} \tag{20}$$

The elastic symmetry error function is formulated as follows:

$$error_{\text{stiff}}(\rho^e, \mathbf{d}) = \frac{error_{\text{stiff}}^{\text{cubic}}(\rho^e, \mathbf{d})}{error_{\text{stiff}}^{\text{norm}}(\rho^e, \mathbf{d})} \tag{21}$$

where $error_{\text{stiff}}^{\text{norm}}$ is a normalization term and $error_{\text{stiff}}^{\text{cubic}}$ places a restriction on all but the three independent elastic stiffness coefficients as follows:

$$error_{\text{stiff}}^{\text{cubic}} = (C_{11}^{\text{H}} - C_{22}^{\text{H}})^2 + (C_{22}^{\text{H}} - C_{33}^{\text{H}})^2 + (C_{44}^{\text{H}} - C_{55}^{\text{H}})^2 + (C_{55}^{\text{H}} - C_{66}^{\text{H}})^2 + (C_{12}^{\text{H}} - C_{13}^{\text{H}})^2 + (C_{12}^{\text{H}} - C_{23}^{\text{H}})^2$$
$$+ \sum_{j=4}^{6} \sum_{i=1}^{j-1} (C_{ij}^{\text{H}})^2 \tag{22}$$

It should be noted that this penalty function differs slightly from functions used in other works. Sigmund and Torquato (1997) consider two-dimensional elasticity and enforce square symmetry by including only diagonal terms in the penalty function; off-diagonal shear terms are not present. Although not explicitly stated, it is presumed that this formulation was extended to three dimensions to obtain the results found in Sigmund (2000) and Bendsøe and Sigmund (2003), with the only additional restriction being placed on C_{13}^{H} and C_{23}^{H}. In other words, the error functions in those works do not include the last term in Eq. (22). When this term was omitted, however, our algorithm yielded materials having nonzero off-diagonal shear terms, materials that were not cubic.

The error penalty function is normalized for consistency when matrix materials with different elastic properties are used. When the error is enforced as a penalty term in the objective function, the normalization function must prevent the effective stiffness tensor from going to a zero matrix when w_{stiff}, the weight assigned to the error function, is very large. Examples of the normalization function from previous works include the square of the partial trace of $\mathbf{C}^{\text{H}}$ (using only the diagonal terms relating normal stress and strain) (Sigmund and Torquato, 1997), and the square of the in-plane bulk modulus (Sigmund et al., 1998).

However, the objective function can be improved by increasing the magnitude of the error normalization term to reduce the error penalty. This was occasionally observed when w_{stiff} was very large and could potentially decrease the elastic design property. We avoid this pitfall by simply using the design objective as the error function normalization term, i.e.,

$$error_{\text{stiff}}^{\text{norm}} = (B^{\text{H}}(\rho^e, \mathbf{d}))^2 \tag{23}$$

Although we present results only for cubic maximum bulk modulus materials in this paper, the approach is easily extended to any symmetry or elastic property that can be expressed as a function of the elasticity tensor (e.g., Young's modulus, Poisson's ratio, etc.).

3.2. The permeability term in the objective function

The objective with respect to fluid transport will be to design a periodic material with maximum permeability and isotropic flow symmetries. By definition, the isotropic permeability tensor must take the form:

$$\mathbf{K}^{\text{H}} = k^{\text{H}} \mathbf{I} \tag{24}$$

where k^{H} is the scalar permeability and is computed by

$$k^{\text{H}} = \frac{1}{d} \sum_{i=1}^{d} K_{ii}^{\text{H}} \tag{25}$$

The permeability function to be optimized is therefore given by the following expression:

$$f_{\text{perm}}(\rho^e, \mathbf{w}) = \frac{k^{\text{H}}(\rho^e, \mathbf{w})}{k^*} \tag{26}$$

where we have chosen the normalization term k^* to be the maximum permeability, which can be found by solving problem (16) with $\alpha_{\text{perm}} = 1$ (and without normalization).

To enforce isotropy, the flow penalty function $error_{\text{perm}}$ is computed by the following expression:

$$error_{\text{perm}}(\rho^e, \mathbf{w}) = \frac{error_{\text{perm}}^{\text{iso}}(\rho^e, \mathbf{w})}{error_{\text{perm}}^{\text{norm}}(\rho^e, \mathbf{w})} = \frac{\sum_{i=1}^{d-1} \left(K_{ii}^{\text{H}} - K_{(i+1)(i+1)}^{\text{H}} \right)^2 + \sum_{i=1}^{d} \sum_{j=i+1}^{d} (K_{ij}^{\text{H}})^2}{error_{\text{perm}}^{\text{norm}}(\rho^e, \mathbf{w})} \tag{27}$$

where the normalization expression $error_{\text{perm}}^{\text{norm}}$ is chosen to be the square of the scalar permeability k^{H}, preventing the algorithm from yielding zero permeability designs when w_{perm} is very large.

Although maximum isotropic permeability is the only case considered here, extension of the methodology to other permeability objectives and symmetries is straightforward. For such other design problems, the error normalization term could be the square of the property to be maximized or the trace of $\mathbf{K}^{\text{H}}$.

4. Known numerical implementation issues

Problem (16) is extraordinarily complex and difficult to solve. First, it is a binary, moving-boundary optimization problem due to the binary design variable constraint and no-slip condition along the solid–fluid interface. As such, direct solution is an extremely difficult task requiring discrete optimization algorithms and updating the nodal boundary conditions representing the no-slip condition at every design iteration. A second complexity is that the maximum stiffness problem is ill-posed (Tartar, 1977; Lurie et al., 1982; Kohn and Strang, 1986). While it was recently determined that the fluid optimization problem is well posed (Borrvall and Petersson, 2003; Evgrafov, 2005) it is not yet known under what combinations of α_{stiff} and α_{perm} the combined problem will be well posed.

The following sections describe the numerical techniques we use for circumventing known numerical instabilities and difficulties in the individual stiffness and flow problems, respectively.

4.1. Regularizing the optimization problem

Due to the inherent difficulty of binary programming problems, it is common practice in structural optimization to relax the 0–1 constraint on ρ^e, transforming the problem into a continuous material distribution problem. Although permitted, elements with intermediate volume fractions (between ρ_{min}^e and 1) are undesirable and are thus penalized to limit their presence in the final solution. This penalization is applied to element stiffness matrices as opposed to an explicit term in the objective function. For the fluid problem, the penalization is directly tied into the regularization of the moving-boundary no-slip condition.

4.1.1. Regularization of the stiffness problem

With respect to the elastic problem, we use the popular SIMP method (solid isotropic material with penalization) developed by Bendsøe (1989) for the penalization. SIMP raises the volume fraction coefficient of element stiffness tensors to the exponent η, meaning Eq. (17) is replaced with

$$\mathbf{k}^e(\rho^e) = (\rho^e)^{\eta} \mathbf{k}_0^e \tag{28}$$

where $\eta > 1$, thereby decreasing the stiffness of elements with intermediate ρ^e, making them uneconomical. To avoid local minima, a continuation method is used where η is initially small and raised in subsequent design iterations as described in Guest et al. (2004). The reader is referred to Bendsøe and Sigmund (2003) for more detail on the SIMP and continuation methods.

4.1.2. Regularization of the fluid flow problem

Regularization of the no-slip condition and binary constraint on ρ^e in fluid topology optimization is a topic that has only recently been studied. Proposed techniques for Stokes flow optimization problems, which are the governing equations in the fluid homogenization problem, penalize nodal velocities of solid elements to

approximate the no-slip condition. These techniques include using a numerical damping term derived from a plane flow model (Borrvall and Petersson, 2003) and using variable viscosity or two material phases with high and low permeability (Evgrafov, 2005). We prefer a Darcy flow regularization developed by the authors where the solid phase is treated as a porous medium and consequently flow "through" the solid phase is governed by Darcy's law. Nodal velocities can then be driven to zero by assigning a low value to the solid phase permeability κ. The advantages of this approach are that it is straightforward, uses existing stabilized finite element formulations to solve the Darcy–Stokes flow problem, and offers the potential for optimizing the layout of a permeable solid phase as Darcy's law would govern flow in such a case. Further, the binary constraint is relaxed yet 0–1 designs can be achieved without additional penalization of intermediate volume fractions. The numerical implementation of the Darcy regularization is summarized here, though the reader is referred to Guest and Prévost (2006) for details.

Treating the solid phase as a porous medium means that various regions in the design domain will be governed by different equations. This discontinuity can be eliminated by combining the equations through the binary material distribution function ρ, creating the following Darcy–Stokes system of equations that governs flow everywhere in the domain:

$$\left((1 - \rho(\mathbf{y}))\nabla^2 - \rho(\mathbf{y})\frac{1}{\kappa}\mathbf{I} \right)\mathbf{w}^{(i)}(\mathbf{y}) - \nabla\pi^{(i)}(\mathbf{y}) = -\mathbf{e}^{(i)} \quad \mathbf{y} \in \Omega(Y)$$
$$\nabla \cdot \mathbf{w}^{(i)}(\mathbf{y}) = 0 \quad \mathbf{y} \in \Omega(Y) \tag{29}$$

Note that the explicit no-slip condition no longer appears but rather is simulated by using a low value of the solid phase permeability κ.

A primary advantage of the Darcy regularization is that it allows for consistency with the aforementioned solution of the Stokes equations. The Darcy flow component of Eq. (29) is also solved numerically in mixed formulation using stabilized finite elements to circumvent the Babuska–Brezzi condition. Let us give the matrix form of the stabilized Darcy–Stokes flow problem as

$$\begin{bmatrix} \mathbf{K}_{ds}(\rho^e) & -\mathbf{G}_{ds}(\rho^e) \\ \mathbf{G}_{ds}^T(\rho^e) & \mathbf{M}_{ds}(\rho^e) \end{bmatrix} \begin{bmatrix} \mathbf{w}^{(i)} \\ \pi^{(i)} \end{bmatrix} = \begin{bmatrix} \mathbf{f}_{ds}^{(i)}(\rho^e) \\ \mathbf{h}_{ds}(\rho^e) \end{bmatrix} \quad \text{for } i = 1, d \tag{30}$$

where the combined Darcy–Stokes viscosity matrix $\mathbf{K}_{ds}$, gradient matrix $\mathbf{G}_{ds}$, divergence matrix $\mathbf{G}_{ds}^T$, and stabilization matrix $\mathbf{M}_{ds}$ are assembled from Stokes (denoted by s) and Darcy (denoted by d) element matrices in the following manner:

$$\mathbf{K}_{ds}(\rho^e) = \underset{e}{A}\, \mathbf{k}_{ds}^e(\rho^e) = \underset{e}{A} \left((1 - \rho^e + \rho^e_{min})\mathbf{k}_s^e + (\rho^e - \rho^e_{min})\mathbf{k}_d^e \right)$$
$$\mathbf{G}_{ds}(\rho^e) = \underset{e}{A} \left((1 - \rho^e + \rho^e_{min})\mathbf{G}_s^e + (\rho^e - \rho^e_{min})\mathbf{G}_d^e \right)$$
$$\mathbf{G}_{ds}^T(\rho^e) = \underset{e}{A} \left((1 - \rho^e + \rho^e_{min})(\mathbf{L}_s^e + \mathbf{G}_s^{eT}) + (\rho^e - \rho^e_{min})\mathbf{G}_d^{eT} \right) \tag{31}$$
$$\mathbf{M}_{ds}(\rho^e) = \underset{e}{A} \left((1 - \rho^e + \rho^e_{min})\mathbf{M}_s^e + (\rho^e - \rho^e_{min})\mathbf{M}_d^e \right)$$

where $\underset{e}{A}$ is the standard finite element assembly routine. In other words, void elements have Stokes stiffness, solid elements have Darcy stiffness, and elements with intermediate volume fractions have a linearly weighted combination of Stokes and Darcy stiffness. The right-hand side forces $\mathbf{f}_{ds}^i$ and $\mathbf{h}_{ds}$ are computed in the same manner.

We use the Stokes flow and Darcy flow stabilization techniques of Hughes et al. (1986) and Masud and Hughes (2002), respectively. These are convenient because they each allow for equal-order interpolations of the velocity and pressure fields.

Eq. (31) are modified slightly from the original work to account for ρ^e_{min}. In fluid optimization, ρ^e is permitted to obtain the bounds of zero (and one) without losing positive definiteness of the global stiffness matrix. Topology optimization of structures, however, requires a small nonzero minimum allowable volume fraction to prevent singularity. Therefore, Eq. (31) is formulated so that voids maintain exact Stokes stiffness while solid elements have an insignificant portion of Stokes stiffness. Note that solid element nodal velocities are irrelevant, so long as they approach zero.

The linear scaling of the stiffness matrices (Eq. (31)) means solutions will naturally approach 0–1 topologies. The Darcy component dominates the $\mathbf{k}_{ds}^e$ element stiffness computation and therefore greatly reduces cor-

responding nodal velocities for low values of solid phase permeability. The only way to eliminate the Darcy component is for the element to be a true void ($\rho^e = \rho^e_{\min}$). When the volume of voids is limited, intermediate volume fractions are considered 'uneconomical' and 0–1 solutions are achieved without further penalization.

The effective homogenization tensor is now computed by any of the following formulas:

$$\mathbf{K}^{\mathrm{H}} = [K^{\mathrm{H}}_{ij}] = \left[\left\langle w^{(i)}_j \right\rangle\right] = \frac{1}{|Y|} \mathbf{w}^{(i)\mathrm{T}} \mathbf{K}_{\mathrm{ds}} \mathbf{w}^{(j)} = \frac{1}{\lfloor Y \rfloor} \sum_{e \in \Omega} (\mathbf{w}^{(i)})^{e\mathrm{T}} \mathbf{k}^e_{\mathrm{ds}} (\mathbf{w}^{(j)})^e \tag{32}$$

The use of the Darcy–Stokes stiffness matrix is acceptable here because we seek a 0–1 topology for the final solution. Therefore, when low values of solid phase permeability are used, the nodal velocities of solid elements will approach zero, meaning Eq. (32) reduces to Eq. (15).

A continuation method is also used for the value of κ to avoid local minima. The problem is first solved with a relatively large value of solid phase permeability, and κ is decreased in subsequent design iterations as described in Guest and Prévost (2006).

4.2. Initial distribution of material

It is common practice in structural optimization to use a uniform distribution of material as the starting topology for the optimization algorithm. This cannot be done in inverse homogenization problems as a uniform distribution contains no microstructural variation and consequently yields a zero gradient in elemental elastic strain energies, fluid powers, and corresponding sensitivities, leading to the optimization algorithm becoming stuck. It is therefore necessary to prevent the topology from achieving a uniform distribution at any time in the optimization algorithm.

The nonuniform initial distribution of material used here expresses element volume fractions as a linear function of the element's distance from the location of the base cell centroid, with the largest volume fractions being assigned to the elements near the centroid. Sigmund (1994a) used random initial distributions in addition to structured initial distributions. However, we found that this was not an option when solving the maximum stiffness problem independently as the algorithm transformed random distributions into uniform distributions after only one or two iterations. This occurs because a uniform distribution often offers improved stiffness while satisfying the prescribed elastic symmetries. Similar behavior was observed when solving the maximum permeability problem (Guest and Prévost, under review).

Although not reported by Sigmund, initial distributions that express element volume fraction as a function of location also transformed into uniform distributions when solving the maximum stiffness problem with no initial penalization of intermediate volume fractions (i.e., when $\eta_{\mathrm{initial}} = 1.0$). This is again due to the fact that a uniform distribution offers improved stiffness and satisfies the prescribed elastic symmetries. Therefore, the exponent η used by the SIMP method must initially be set to a value greater than 1.0 to penalize intermediate volume fractions from the outset and prevent a uniform distribution from developing.

4.3. Imposing a minimum length scale

The reason for imposing a minimum length scale on load-carrying members in the final topology is threefold. First, it provides the designer with a means for addressing manufacturing restrictions on the smallest feature size. Second, it is well known that the continuum form of the maximum stiffness problem is ill-posed, and thus generally lacks solutions. Solutions can be continuously improved by introducing more holes into the topology while keeping the total volume of material constant, leading to the number of microscopic holes becoming unbounded. This instability is reflected in the discretized version of the problem in the form of mesh dependence, where the density of the mesh influences solutions, and nonoptimal checkerboard patterns, or regions of alternating solid and void elements (see e.g., Haber et al., 1996; Sigmund and Petersson, 1998). One approach to eliminating these numerical instabilities is to require load-carrying members in the final topology to achieve a minimum length scale, or minimum size, thereby restricting the design space and ensuring solutions exist to the original continuum problem. This restriction ensures mesh independent and checkerboard-free topologies as local features smaller than the physical length scale are prohibited. Although

the fluid optimization does not exhibit these properties (Borrvall and Petersson, 2003; Evgrafov, 2005), it is not yet known under what combinations of α_{stiff} and α_{perm} the combined problem will be well posed.

The third reason for imposing a minimum length scale is that the maximum bulk modulus problem does not possess a unique solution. Microstructures known to achieve the upper Hashin–Shtrikman bounds include the coated spheres assembly (Hashin, 1961), rank laminates (e.g., Francfort and Murat, 1986), Vigdergauz (1989, 1999) microstructures, and new microstructures presented by Sigmund (2000) and Bendsøe and Sigmund (2003). The work presented here will be limited to single-length-scale microstructures like that of the optimal Vigdergauz structures. This restriction can be achieved by imposing a minimum length scale on structural members that is large relative to the size of the base cell (Bendsøe and Sigmund, 2003).

We use the method of nodal design variables and projection functions developed by Guest et al. (2004) to impose a minimum length scale. This approach uses nodal volume fractions, denoted as ρ_n, as the design variables and projects these variables onto element space via a regularized Heaviside function to determine the element-wise ρ^e that define topology. The technique was shown to yield 0–1, minimum length scale compliant solutions to macroscopic design problems. The approach is summarized here, although the reader is referred to the original work for details.

The underlying idea for this approach is quite simple. Let us define r_{min} as the minimum allowable radius of solid phase members in the final topology. Solid material is assigned to all elements within a distance r_{min} of a node with volume fraction $\rho_n = 1$. Fig. 1a illustrates this idea. This insures that when an element is designated solid it is part of a structural member that is of at least diameter $2r_{\text{min}}$. From the element's perspective, all nodes within a distance r_{min} of the centroid of an element e influence the element's volume fraction ρ^e. This can be visualized by drawing a circular sub-domain Ω_w^e of radius r_{min} around the centroid of e as shown in Fig. 1b. Nodes located inside Ω_w^e contribute to the computation of ρ^e.

The example given above is the binary case. In practice, nodal volume fractions ρ_n are projected onto the element e via the following regularized Heaviside function:

$$\rho^e = 1 - e^{-\beta\mu^e(\rho_n)} + \mu^e(\rho_n)e^{-\beta} \tag{33}$$

where the parameter β dictates the curvature of the regularization, with $\beta = 0$ resulting in a linear regularization and $\beta = \infty$ approaching the Heaviside function. Generally, a continuation method is used such that β is initially chosen to be small and is raised in subsequent iterations to allow convergence to a 0–1 topology. The function $\mu^e(\rho_n)$ is the linear weighted average of the volume fractions of nodes located inside Ω_w^e. The weighting scheme is based on proximity of the node to the element centroid, with nearest nodes receiving the largest weights (Guest et al., 2004).
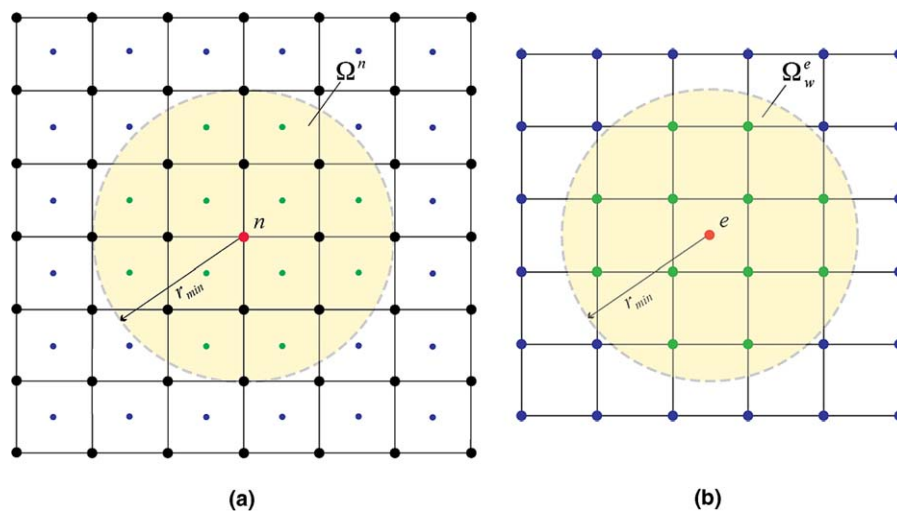

Fig. 1. The domains of influence for the minimum length scale scheme. (a) From the node n's perspective: when ρ_n indicates solid material, all elements having centroid located within a distance r_{min} are designated solid elements. (b) From the element's perspective: when any node within distance r_{min} of the centroid of e indicates solid material, e is a solid element (i.e., nodes located inside Ω_w^e influence ρ^e).
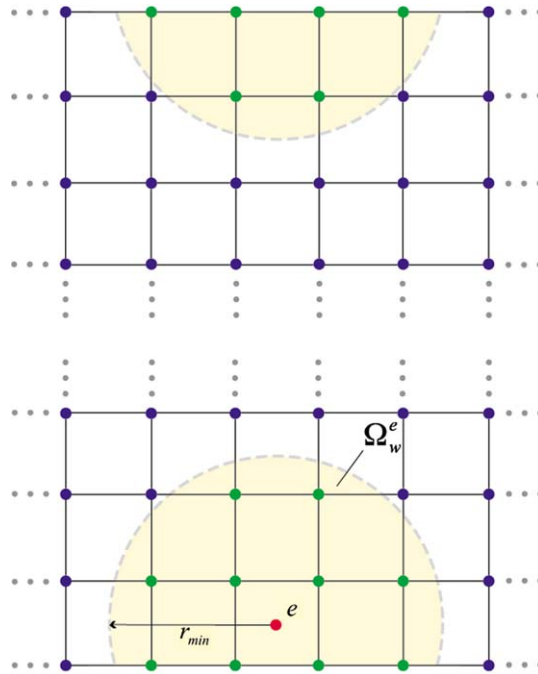
Fig. 2. In periodic materials, minimum length scale is respected across base cell boundaries. Therefore, when the domain Ω_w^e intersects a boundary it is mapped to the opposing boundary of the base cell.

Applying the methodology to periodic materials requires the minimum length scale to be respected across the base cell boundaries. Therefore, when Ω_w^e intersects a boundary it extends into the neighboring base cell, or equivalently into the interior of the same base cell from the opposing boundary. Fig. 2 demonstrates this concept. As the nodal weighting function $\mu^e(\rho_n)$ is based on proximity to the element centroid, auxiliary nodal coordinates corresponding to the location in the neighboring base cell should be used for nodes located in the portion of Ω_w^e that has crossed a boundary. Further, opposing nodes on the boundary should have the same nodal volume fractions. This is achieved simply by assigning the same nodal design variable number to these nodes.

Implementing this technique requires only minor modifications to the original inverse homogenization problem. The element-wise volume fractions ρ^e that define topology are simply expressed as a function of nodal volume fractions ρ_n. The objective function, homogenization constraints, and volume constraint remain the same, while the design variable bounds are applied to ρ_n.

5. The optimization algorithm

The regularized form of problem (16) with minimum length scale control via nodal design variables and projection functions is given as

$$
\max_{\rho_n, \mathbf{d}, \mathbf{w}, \boldsymbol{\pi}} \quad \alpha_{\text{stiff}} f_{\text{stiff}}(\rho_n, \mathbf{d}) + \alpha_{\text{perm}} f_{\text{perm}}(\rho_n, \mathbf{w}) - w_{\text{stiff}}\, error_{\text{stiff}}(\rho_n, \mathbf{d}) - w_{\text{perm}}\, error_{\text{perm}}(\rho_n, \mathbf{w})
$$

$$
\begin{aligned}
\text{subject to} \quad & \mathbf{K}_{\text{stiff}}(\rho_n)\mathbf{d}^{(i)} = \mathbf{f}_{\text{stiff}}^{(i)} \qquad \text{for } i = 1, d(d+1)/2 \\[6pt]
& \begin{bmatrix} \mathbf{K}_{\text{ds}}(\rho_n) & -\mathbf{G}_{\text{ds}}(\rho_n) \\ \mathbf{G}_{\text{ds}}^{\mathrm{T}}(\rho_n) & \mathbf{M}_{\text{ds}}(\rho_n) \end{bmatrix} \begin{bmatrix} \mathbf{w}^{(j)} \\ \pi^{(j)} \end{bmatrix} = \begin{bmatrix} \mathbf{f}_{\text{ds}}^{(j)}(\rho_n) \\ \mathbf{h}_{\text{ds}}(\rho_n) \end{bmatrix} \quad \text{for } j = 1, d \\[6pt]
& V_{\min} \leqslant \sum_{e \in \Omega} \rho^e(\rho_n) v^e \leqslant V_{\max} \\[4pt]
& \rho_n^{\min} \leqslant \rho_n \leqslant 1 \quad \forall n \in \Omega \\[2pt]
& \mathbf{d}^{(i)}, \mathbf{w}^{(j)} \text{ is } Y\text{-periodic}
\end{aligned}
\tag{34}
$$

where $\rho_n^{\min}$ is the minimum allowable nodal volume fraction (Guest et al., 2004).

5.1. Solution scheme

Problem (34) can be solved using a nested approach. Displacements and velocities for the current topology are found by solving the equilibrium equations (5) and (30), respectively. These equations are solved independently as we have assumed fluid velocities are uncoupled from deformation of the matrix material.

Displacements and velocities are then held constant and the optimization problem is solved to determine the new nodal volume fractions ρ_n. Consequently, the fixed displacements and velocities optimization problem reduces to the following, given in minimization form (Guest, 2005):

$$\min_{\rho_n} \quad -\alpha_{\text{stiff}} f_{\text{stiff}}(\rho_n, \mathbf{d}) + \alpha_{\text{perm}} f_{\text{perm}}(\rho_n, \mathbf{w}) + w_{\text{stiff}} \, error_{\text{stiff}}(\rho_n, \mathbf{d}) - w_{\text{perm}} \, error_{\text{perm}}(\rho_n, \mathbf{w})$$

$$\text{subject to} \quad V_{\min} \leqslant \sum_{e \in \Omega} \rho^e(\rho_n) v^e \leqslant V_{\max} \tag{35}$$

$$\rho_n^{\min} \leqslant \rho_n \leqslant 1 \quad \forall n \in \Omega$$

Problem (35) is solved using the method of moving asymptotes (MMA) (Svanberg, 1995), an algorithm that minimizes sequential convex approximations of the original function and is known to be very efficient for structural optimization problems. The convex sub-problem is solved using the interior point method detailed in Benson et al. (2002). The displacements and fluid velocities are updated following each MMA iteration and the process iterates until the topology converges.

5.2. Avoiding pitfalls of the continuation methods

When solving the stiffness and permeability design problems independently, continuation methods allow intermediate volume fractions to exist with little or no penalization during early design iterations. This helps prevent solutions from converging to local minima. As noted, these continuation methods are applied to the exponent penalty in the SIMP method, the solid phase permeability in the Darcy regularization, and the regularized Heaviside parameter β for the minimum length scale scheme.

A shortcoming of this approach was revealed when the combined problem was first solved. By using a relatively high value for the initial material permeability κ, velocities at the nodes of solid elements are not significantly penalized. When weight on the stiffness objective was high, a plane of solid material would form such that it filled an entire cross-section of the base cell before κ was sufficiently decreased. As velocity is held constant during the design iteration in the nested approach, this plane would remain composed of solid elements and permeability in the direction normal to the plane would approach zero. This was not seen in the permeability-only design problem as there was no incentive to improve effective stiffness.

This issue could likely be avoided by using more rigorous and computationally expensive algorithms, such as binary optimization algorithms (without continuation methods) or algorithms that solve the original problem simultaneously for nodal volume fractions, solid displacements, and fluid velocities, rather than by nested approach. Alternatively, one could start with a much smaller initial value for κ to prevent the completely solid cross-section from appearing early in the design iterations, although this would more likely result in solutions that are local minima.

The approach taken here is to require a minimum permeability for the microstructure at early stages of the design. This minimum allowable permeability, $k_{\min}$, should approach zero as the algorithm progresses and the solid phase permeability κ is reduced. Its initial value is chosen to be slightly greater than the effective permeability of a microstructure featuring a thin plane of solid elements blocking flow in each principle direction – i.e., single sheets of solid material lying in the x–y, y–z, and x–z global coordinate planes. Therefore, when the algorithm begins, a temporary dummy vector of element volume fractions is constructed to match this profile and the effective permeability is computed using the initial value of κ. This effective permeability is increased slightly (e.g., 1%) and assigned to $k_{\min}$. It is sufficient for our purposes to assume that the velocity in solid elements is proportional to the material permeability κ (Guest and Prévost, 2006), and thus the fictitious topology does not need to be analyzed again. In future iterations, when κ is decreased, $k_{\min}$ is decreased proportionally.

The minimum permeability constraint is imposed as a penalty in the objective function. Denoted as $S_{k\min}$, its magnitude must be very large when $k^H < k_{\min}^H$, and near-zero otherwise. There are many well-known barrier

functions that exhibit these characteristics. However, the authors have used the following penalty function in other work (Guest, 2005) and so it is used here out of convenience:

$$S_{k\min}(\rho_n, \mathbf{w}) = \left((1 + k_{\min}^{\mathrm{H}} - \zeta_1)\left(1 - \frac{k^{\mathrm{H}}(\rho_n, \mathbf{w})}{k^*}\right)\right)^{\zeta_2} \tag{36}$$

where ζ_1 and ζ_2 control the location and slope of the penalty curve, respectively (Guest, 2005). Note that function is zero when the effective permeability achieves the upper bound ($k^{\mathrm{H}} = k^*$).

As we are operating with fixed nodal velocities, the penalty term $S_{k\min}$ is subtracted from the objective function of Problem (35). This implementation has been successful in preventing the design of microstructures that prematurely block flow with solid elements, while seeming to have little to no impact on problems where flow should be blocked (α_{stiff} near 1) or where flow is not ever blocked (large α_{perm}).

6. Designs for 3-D periodic materials with maximized stiffness and permeability

It is not possible to design microstructures with optimized stiffness and fluid transport properties in a two-dimensional setting if square elastic and/or isotropic fluid flow symmetries are desired. Non-zero elastic stiffness would require a continuous body of material to connect opposing boundaries of the base cell, thereby eliminating macroscopic flow in the direction parallel to those boundaries. The combined problem is therefore only solved in three dimensions.

The results contained in this section were produced using a cube design domain of unit volume with the prescribed volume of material equal to 0.50 ($V_{\min} \approx 0.5 \approx V_{\max}$). Young's modulus of the matrix material is arbitrary and is thus set to 1, Poisson's ratio is 0.33, and $r_{\min}$ is 0.05. As for the parameters affected by the continuation methods, β of the element projection functions is initially 10, exponent η of the SIMP method is initially 5.0, and material permeability κ is initially $0.042h^2$, slightly lower than the permeability at which the diagonal terms of the Darcy and Stokes viscosity stiffness matrices are equal for an 8-node cube. The problem was solved using 8-node brick elements with the minimum permeability penalty function enabled.

The results shown in this section are designs for three-dimensional periodic materials with maximized bulk modulus B^{H} and permeability k^{H}. The elastic symmetry requirement is cubic while flow is required to be isotropic, with each penalty function assigned equal weight ($w_{\mathrm{stiff}} = w_{\mathrm{perm}}$). The problem was solved for the following weight combinations:

(a) $\alpha_{\mathrm{stiff}} = 1.00$ $\alpha_{\mathrm{perm}} = 0.00$ (b) $\alpha_{\mathrm{stiff}} = 0.75$ $\alpha_{\mathrm{perm}} = 0.25$
(c) $\alpha_{\mathrm{stiff}} = 0.50$ $\alpha_{\mathrm{perm}} = 0.50$ (d) $\alpha_{\mathrm{stiff}} = 0.25$ $\alpha_{\mathrm{perm}} = 0.75$
(e) $\alpha_{\mathrm{stiff}} = 0.00$ $\alpha_{\mathrm{perm}} = 1.00$

Fig. 3 displays the periodic material structures that result under the weighting schemes. The periodic structures shown are composed of eight base cells. Details of the material microstructure can be seen in Fig. 4, which displays the solid phase of the base cells and corresponding periodic material structures. The topology of the fluid phase corresponding to these base cells is difficult to interpret. Therefore, a new base cell was extracted from the periodic structures such that the center of the new base cell is located at the corner of the base cells shown in Fig. 4. The fluid phase of these new base cells and corresponding periodic materials are shown in Fig. 5. Note that the periodic structures shown in Fig. 5 are located $(0.5, 0.5, 0.5)$ from the periodic structures shown in Fig. 4.

When only stiffness is optimized (case a), the base cell design is a hollow box with rounded corners, resembling cubic maximum bulk modulus designs previously reported in literature (Sigmund, 2000; Bendsøe and Sigmund, 2003). The box design is a close-walled structure and consequently the effective permeability is zero. This is clearly shown by the cross-section view in Fig. 5a as the fluid base cells are disconnected from one another.

When the weight on the permeability term in the objective function increases to 0.25, small rectangular holes develop in the periodic material, forming channels for fluid flow as shown in Fig. 4b. As the importance of permeability rises, the diameter of the channel at its narrowest point becomes larger, allowing more fluid to pass through the material. The shape of the channel also improves flow efficiency as it changes from a
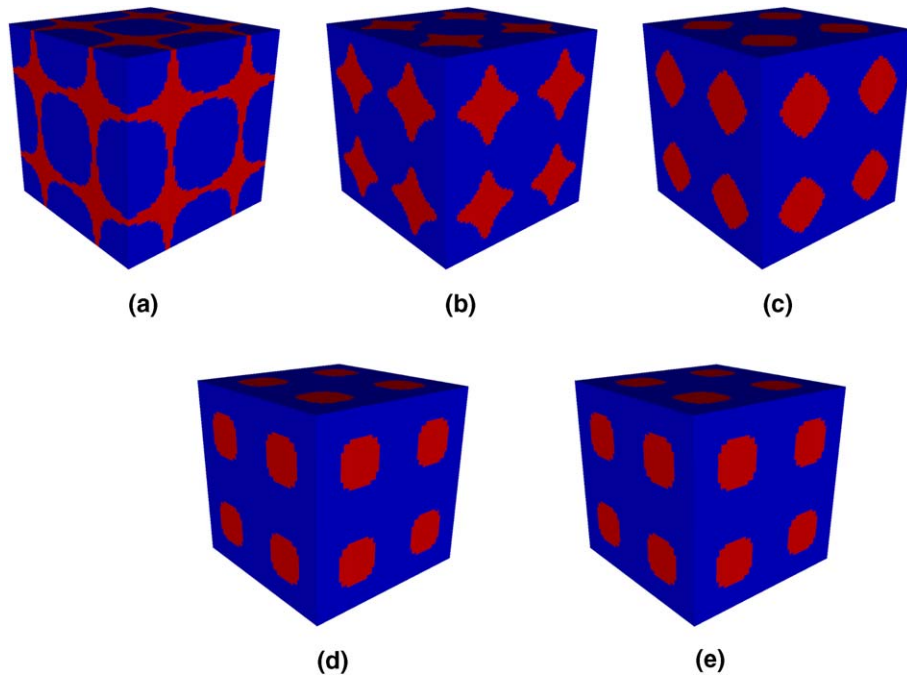
Fig. 3. Optimal periodic structures for the following weighting schemes: (a) $\alpha_{\text{stiff}} = 1.00$, $\alpha_{\text{perm}} = 0.00$; (b) $\alpha_{\text{stiff}} = 0.75$, $\alpha_{\text{perm}} = 0.25$; (c) $\alpha_{\text{stiff}} = 0.50$, $\alpha_{\text{perm}} = 0.50$; (d) $\alpha_{\text{stiff}} = 0.25$, $\alpha_{\text{perm}} = 0.75$; and (e) $\alpha_{\text{stiff}} = 0.00$, $\alpha_{\text{perm}} = 1.00$. Each periodic structure is composed of eight base cells.

rectangular cross-section for $\alpha_{\text{perm}} = 0.25$ and $\alpha_{\text{perm}} = 0.50$ to a circular cross-section for $\alpha_{\text{perm}} = 0.75$ and $\alpha_{\text{perm}} = 1.00$ (see Fig. 4). This is also clearly demonstrated in Fig. 5 as the fluid connectivity between the base cells become larger and more circular as α_{perm} increases.

Another noticeable change as α_{perm} increases from zero and α_{stiff} decreases from one is that the edges of the hollow box design become smoother as material is moved from the edges of the base cell towards the center. This decreases mechanical stiffness but also decreases the area of the solid–fluid interface where velocities are zero due to the no-slip condition, thereby improving permeability. From the perspective of the fluid phase (Fig. 5), the topology changes from a circular ball to a smooth, more pipe-like design.

For the case of $\alpha_{\text{perm}} = 1.00$ (case e), where permeability is the only property being optimized, the base cell resembles the Schwarz P minimal surface as reported by the authors (Guest, 2005; Guest and Prévost, under review). This is a logical design as it minimizes the solid-fluid interface where velocities are zero. It is interesting to note, however, that this minimal surface offers some mechanical stiffness ($B^{\text{H}} = 0.163$). This is unlike the maximum stiffness design that yields zero permeability.

The computed bulk modulus and permeability values for the presented material structures are summarized in Table 1. Optimality of the microstructures is verified by comparing the computed properties to known property bounds. The Hashin–Shtrikman theoretical upper bound on bulk modulus for an isotropic material with phases and void ratio used here is 0.253. This is slightly above the computed bulk modulus for case (a) of 0.240, with the difference likely due to operating on a relatively coarse mesh and restricting the design space to single length scale microstructures. As mentioned above, the Schwartz P minimal surface is believed to be the maximum permeability structure. The corresponding permeability (case e) is computed as 3.18×10^{-3}, which compares reasonably well with the permeability of the Schwartz P minimal surface computed by Jung and Torquato (2005) ($k^{\text{H}} = 3.48 \times 10^{-3}$). The difference in magnitude is due to operating on a *much* coarser mesh than Jung and Torquato, thereby reducing accuracy and, more importantly, limiting the degree of smoothness the microstructure can obtain. The mesh used here is necessarily coarser as we are solving a multi-physics problem and are operating in the context of iterative design, rather than simply analysis.
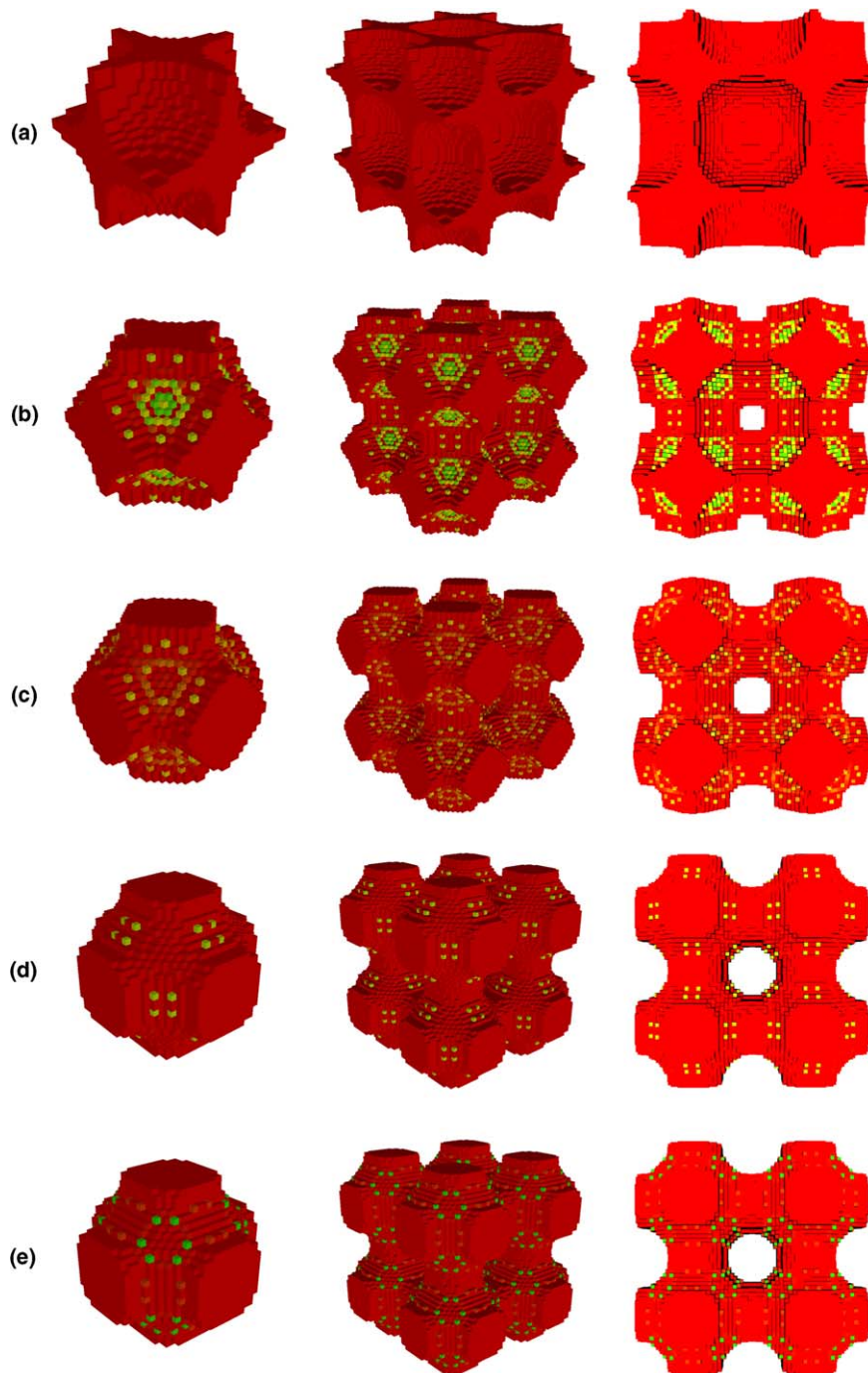
Fig. 4. The solid phase base cell (left), periodic structure (center), and periodic structure cross-section (right) corresponding to the designs shown in Fig. 3 for the five weight cases.

With the exception of case (d), the property magnitudes given in Table 1 also follow the expected trend. As shown in Figs. 4 and 5, the designs for case (d) and (e) are nearly identical. Although the permeability of design (d) is slightly lower as expected, the bulk modulus is also lower, despite a larger weight assigned to the stiffness term in the objective function. This suggests the result for case (d) is not the global optimum
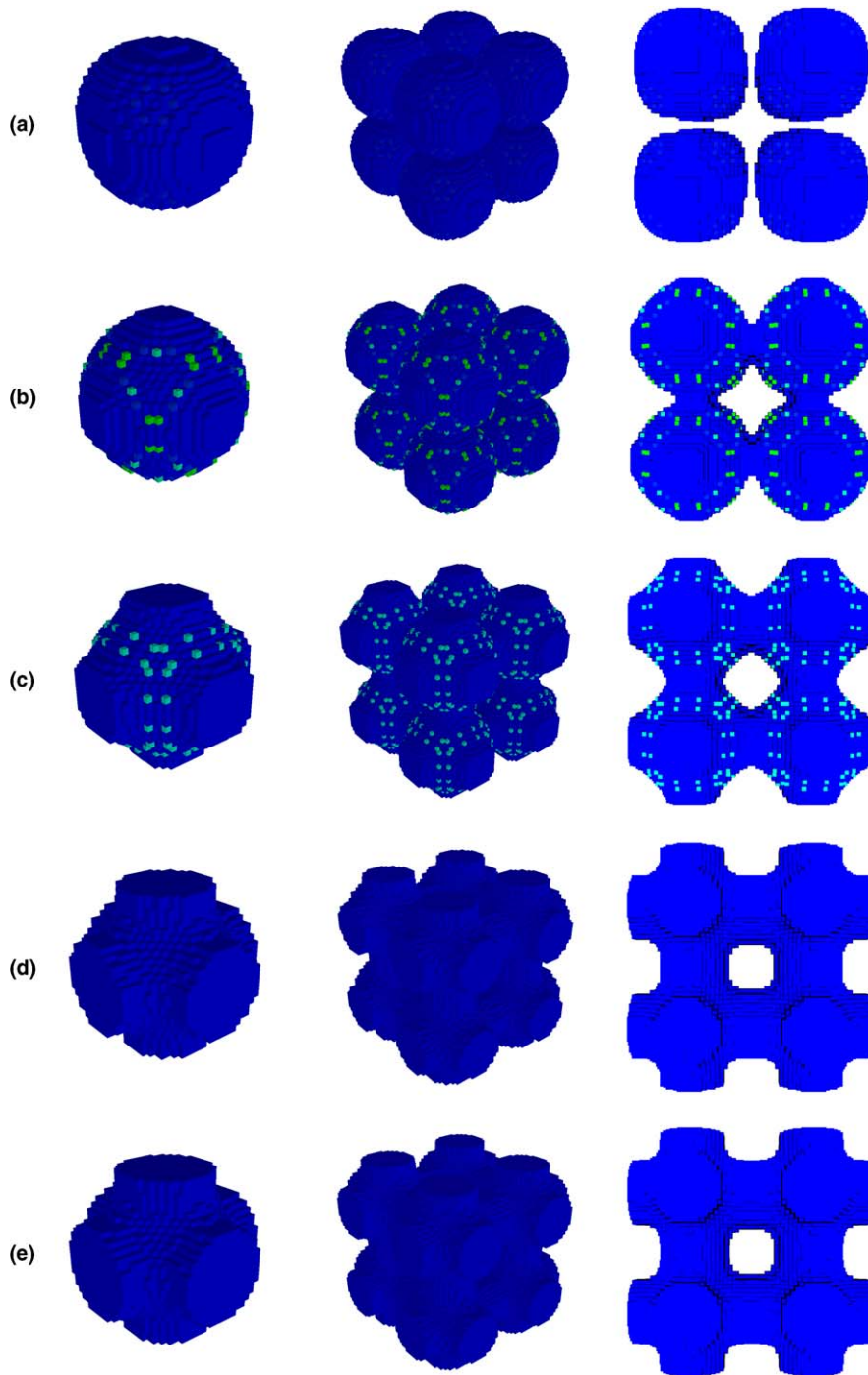
Fig. 5. The fluid phase base cell (left), periodic structure (center), and periodic structure cross-section (right) corresponding to the designs shown in Fig. 3 for the five weight cases. In order to clearly illustrate topology, these base cells were extracted from the corners of the base cells of Fig. 4. In other words, the periodic structures shown here are located (0.5, 0.5, 0.5) from the periodic structures shown in Fig. 4.

and is instead a local minimum. It is also likely that operating on a relatively coarse $30 \times 30 \times 30$ element mesh has contributed to this aberration and that finer meshes, while not guaranteeing global minima, will make local minima less evident.

Table 1
Effective bulk modulus and permeability for the periodic materials created under the various weighting schemes

	Case				
	(a)	(b)	(c)	(d)	(e)
α_{stiff}, α_{perm}	1.00, 0.00	0.75, 0.25	0.50, 0.50	0.25, 0.75	0.00, 1.00
B^H	0.240	0.200	0.179	0.161	0.163
k^H (10^{-2})	9.53e-4	0.0677	0.213	0.300	0.318

Note: Elastic and flow symmetries were negligible for all cases $\left(\sqrt{error_{stiff}^{cubic}} < 10^{-6} \text{ and } \sqrt{error_{perm}^{iso}} < 10^{-12} \right)$.

7. Concluding remarks

This paper proposes a topology optimization methodology for designing multifunctional porous material microstructures optimized for stiffness and fluid permeability. As these are competing properties, the problem was formulated such that designs are dependent upon the weight, or relative importance, assigned to the stiffness and transport terms in the objective function. The designer selects these values based on the materials future use, thus allowing the microstructure to be tailored according to its specific application.

Achieving these designs required simultaneous solution of elastic and fluid transport inverse homogenization problems, a complex task given that they are governed by vector equations and must be solved in three-dimensional space. Inherent numerical instabilities of the maximum stiffness problem were overcome by imposing a minimum length scale on structural features via the nodal design variable and projection function technique (Guest et al., 2004). This also provides a means for satisfying manufacturing constraints. Numerical difficulties associated with the binary, moving-boundary fluid transport optimization problem were overcome via a Darcy flow regularization procedure (Guest and Prévost, 2006).

A drawback of the proposed algorithm is the reliance on parameters in the stiffness and flow regularizations and associated continuation methods. It is possible that these schemes will need tuning when introducing new physics into the combinatorial optimization problem. However, the parameter magnitudes and continuation schemes used here are nearly identical to those used when solving the individual physics problems for which they were originally developed. The regularization and continuation method parameters can be removed by replacing the presented nested-loop, continuous optimization algorithm with a discrete optimization algorithm that simultaneously solves for the design and state variables. This, however, would increase computational demands immensely and increase the probability of solutions being local and not global minima.

The methodology was successfully used to design three-dimensional periodic materials having maximized bulk modulus and permeability while exhibiting cubic elastic and isotropic flow symmetries. Figs. 4 and 5 and Table 1 illustrate the advantage of the multi-objective methodology as the prescribed weighting schemes clearly influenced design. The results presented here consider just five combinations of weights. Obviously, a wide-range of designs can be achieved by considering more combinations, although a finer mesh is likely required to see more subtle changes in topology.

Although bulk modulus and isotropic permeability were the only material properties presented here, the methodology can be extended to optimize any combination of elastic and flow properties and symmetries. This would include optimizing Young's modulus, shear modulus, or multiple elastic properties while requiring lower bounds on flow material properties. If the material orientation is known, directional stiffness and flow properties could also be optimized.

It is important to emphasize that the underlying methodology of inverse homogenization via topology optimization is quite general and can be applied to the design of composite materials. Further, other material properties of interest (e.g., thermal conductivity or expansion, electrical conductivity, etc.) can be substituted or added to the presented combinatorial design optimization problem.

Acknowledgements

References

Babuska, I., 1971. Error bounds for finite element method. Numerische Mathematik 16, 322–333.

Bendsøe, M.P., 1989. Optimal shape design as a material distribution problem. Structural Optimization 1, 193–202.

Bendsøe, M.P., Kikuchi, N., 1988. Generating optimal topologies in structural design using homogenization method. Computer Methods in Applied Mechanics and Engineering 71, 197–224.

Bendsøe, M.P., Sigmund, O., 2003. Topology Optimization: Theory, Methods and Applications. Springer, Berlin.

Benson, H.Y., Shanno, D.F., Vanderbei, R.J., 2002. Interior-point methods for nonconvex nonlinear programming: filter methods and merit functions. Computational Optimization and Applications 23, 257–272.

Bensoussan, A., Lions, J.L., Papanicolaou, G., 1978. Asymptotic Analysis for Periodic Structures. North-Holland, Amsterdam.

Borrvall, T., Petersson, J., 2003. Topology optimization of fluids in Stokes flow. International Journal for Numerical Methods in Fluids 41, 77–107.

Brezzi, F., 1974. On the existence, uniqueness and approximation of saddle-point problems arising from Lagrange multipliers. Rev. Francaise d'Automatique Inform. Recherche Operationnelle 8 (R-2), 129–151.

Evgrafov, A., 2005. The limits of porous materials in topology optimization of Stokes flows. Applied Mathematics and Optimization 52, 263–277.

Francfort, G.A., Murat, F., 1986. Homogenization and optimal bounds in linear elasticity. Archive for Rational Mechanics and Analysis 94, 307–334.

Guedes, J.M., Kikuchi, N., 1990. Preprocessing and postprocessing for materials based on the homogenization method with adaptive finite element methods. Computer Methods in Applied Mechanics and Engineering 83, 143–198.

Guest, J.K., 2005. Design of optimal porous material structures for maximized stiffness and permeability using topology optimization and finite element methods. Ph.D. dissertation. Princeton University.

Guest, J.K., Prévost, J.H., 2006. Topology optimization of creeping fluid flows using a Darcy-Stokes finite element. International Journal for Numerical Methods in Engineering 66, 461–484.

Guest, J.K., Prévost, J.H., under review. Design of maximum permeability material structures. Computer Methods in Applied Mechanics and Engineering.

Guest, J.K., Prévost, J.H., Belytschko, T., 2004. Achieving minimum length scale in topology optimization using nodal design variables and projection functions. International Journal for Numerical Methods in Engineering 61, 238–254.

Haber, R.B., Jog, C.S., Bendsøe, M.P., 1996. A new approach to variable-topology shape design using a constraint on perimeter. Structural Optimization 11, 1–12.

Hashin, Z., 1961. Elastic moduli of heterogeneous materials. ASME-Papers, Paper No. 61-WA-39.

Hassani, B., Hinton, E., 1998. A review of homogenization and topology optimization II – Analytical and numerical solution of homogenization equations. Computers and Structures 69, 719–738.

Hughes, T.J.R., Franca, L.P., Balestra, M., 1986. A new finite element formulation for computational fluid dynamics. V. Circumventing the Babuska–Brezzi condition: a stable Petrov–Galerkin formulation of the Stokes problem accommodating equal-order interpolations. Computer Methods in Applied Mechanics and Engineering 59, 85–99.

Jung, Y., Torquato, S., 2005. Fluid permeabilities of triply periodic minimal surfaces. Physical Review E 72, 056319(8).

Kohn, R.V., Strang, G., 1986. Optimal design and relaxation of variational problems. Communications on Pure and Applied Mathematics 39, 1, 25 (I), 139–182 (II), 353–377 (III).

Lurie, K.A., Cherkaev, A.V., Fedorov, A.V., 1982. Regularization of optimal design problems for bars and plates. Journal of Optimization Theory and Applications 37 (4), 499, 522 (I),523-543 (II).

Masud, A., Hughes, T.J.R., 2002. A stabilized mixed finite element method for Darcy flow. Computer Methods in Applied Mechanics and Engineering 191, 4341–4370.

Sanchez-Palencia, E., 1980. Non-homogeneous Media and Vibration TheoryLecture Notes in Physics, vol. 127. Springer, Berlin.

Sigmund, O., 1994a. Design of material structures using topology optimization. Ph.D. dissertation. Technical University of Denmark.

Sigmund, O., 1994b. Materials with prescribed constitutive parameters: an inverse homogenization problem. International Journal of Solids and Structures 31, 2313–2329.

Sigmund, O., 1995. Tailoring materials with prescribed elastic properties. Mechanics of Materials 20, 351–368.

Sigmund, O., 2000. A new class of extremal composites. Journal of Mechanics and Physics of Solids 48, 397–428.

Sigmund, O., Petersson, J., 1998. Numerical instabilities in topology optimization: a survey on procedures dealing with checkerboards, mesh-dependencies and local minima. Structural Optimization 16, 68–75.

Sigmund, O., Torquato, S., 1997. Design of materials with extreme thermal expansion using a three-phase topology optimization method. Journal of Mechanics and Physics of Solids 45, 1037–1067.

Sigmund, O., Torquato, S., Aksay, I.A., 1998. On the design of 1–3 piezocomposites using topology optimization. Journal of Materials Research 13, 1038–1048.

Svanberg, K., 1995. A globally convergent version of MMA without linesearch. In: Rozvany, G.I.N., Olhoff, N. (Eds.), Proceedings of the First World Congress of Structural and Multidisciplinary Optimization, pp. 9–16.

Tartar, L., 1977. Estimation de coefficients homogeneisesLecture Notes is Mathematics, vol. 704. Springer-Verlag, Berlin, pp. 364–373.

Torquato, S., 2002. Random Heterogeneous Materials: Microstructure and Macroscopic Properties. Springer, New York.

Torquato, S., Hyun, S., Donev, A., 2002. Multifunctional composites: optimizing microstructures for simultaneous transport of heat and electricity. Physical Review Letters 89, 266601-1–266601-4.

Torquato, S., Hyun, S., Donev, A., 2003. Optimal design of manufacturable three-dimensional composites with multifunctional characteristics. Journal of Applied Physics 94, 5748–5755.

Vigdergauz, S.B., 1989. Regular structures with extremal elastic properties. Mechanics of Solids 24, 57–63.

Vigdergauz, S.B., 1999. Energy-minimizing inclusions in a planar elastic structure with macroisotropy. Structural Optimization 17, 104–112.